Chinese Chemical Letters 34 (2023) 107858

Contents lists available at ScienceDirect

Chinese Chemical Letters

journal homepage: www.elsevier.com/locate/cclet

One-pot synthesis of bimetallic Fe/Co incorporated silica hollow spheres with superior peroxidase-like activity

Wenli Zhao[a,1], Wenhao Wang[a,1], Fancang Meng[a], Yang Du[b,*], Qingmin Ji[a,*], Heng-Dao Quan[c]

[a] Herbert Gleiter Institute for Nanoscience, School of Materials Science and Engineering, Nanjing University of Science & Technology, Nanjing 210094, China
[b] School of Chemical Engineering, Nanjing University of Science and Technology, Nanjing 210094, China
[c] School of Chemistry and Chemical Engineering, Beijing Institute of Technology, Beijing 100081, China

ARTICLE INFO

Article history:
Received 27 May 2022
Revised 9 August 2022
Accepted 26 September 2022
Available online 29 September 2022

Keywords:
Bimetallic doping
Mesoporous silica
Hollow sphere
Supported catalyst
Peroxidase-like activity

ABSTRACT

Mesoporous silica hollow spheres with a homogenous and high content distribution of Fe and Co were synthesized by a facile one-pot hydrothermal process. The sub-nanometer bimetallic components inside the silica framework facilitate the stable fixation and the open accessibility to active sites. The co-doped Fe/Co in the spheres showed excellent peroxidase-like activity and much higher catalytic performance than their monometallic-supported spheres. The synergistic effect between Fe and Co promotes the continuous formation of functional radicals during the oxidation process and thus accelerates the reaction rate. When used for colorimetric detection of hydrogen peroxide (H_2O_2), the Fe/Co incorporated silica hollow spheres show the capability of detection of H_2O_2 in a wide range (10-250 μmol/L) and with the low detection limit of 0.012 ppm.

The incorporation of metals in mesoporous silica is one of the most effective pathways to bring function to inert silica structures [1,2]. The doped metals may serve as active nano-catalysts for diverse processes, including dehydrogenation of propane [3], hydrogenation of amides [4], acetylene hydrochlorination [5], CO_2 methanation [6], oxidation of organic pollutants [7], and glucose oxidation [8].

To achieve controllable incorporation and stable fixation of metals in silica, it is essential to adjust the structural relationship between supports and metals. One obstacle in the fabrication processes is how to keep the hollow space of the support with the accessibility of active sites. The loading of metals by post-adsorption of metal species in mesoporous silica is the most used strategy [9–11]. However, it may easily cause the formation of large metal particles and partial blocking of the porous spaces or unfavorable aggregations during usage, which may lead to a decrease in catalytic activity and stability. Therefore, fabrication of active metal-loaded mesoporous silica with a high dispersion state is not an easy task. It is also more challenging to incorporate multi-metals in silica, which are prospective for further enhancement of catalytic performance due to synergistic effects [12,13].

Here, we successfully fabricated newly bimetallic incorporated silica hollow spheres of Fe-Co@SHSs by facile one-pot hydrothermal process (Fig. 1a). The distribution state of Fe and Co components within the silica matrix is different from other reported metal-loaded silica spheres. The stable incorporation in the silica framework and porous feature of the silica spheres may facilitate the access of active Fe/Co to external molecules. We analyzed the synergistic effect of metals by comparing the peroxidase-like activity of Fe-Co@SHS with the monometallic doped silica of Fe@SHS or Co@SHS. In addition, a novel colorimetric detection system for H_2O_2 was constructed based on Fe-Co@SHS.

The incorporation of Fe and Co in silica spheres was through integrating two metal species during the dissolution-regrowth process of silica in $NaBH_4$ solution. The process may lead to the formation of porous silica frameworks with plenty of structural defects and silanol groups [14,15]. The metal ions added in the process are inclined to adsorb on the negatively charged silicate species and occur oxidation with the regrowth of silica networks [16,17]. From our previous study, the doped metal amounts and states may lead to different catalytic efficiencies of the hollow spheres [17]. The optimal loading concentration is 1 mmol/L, which resulted in the doping amount of about 6 wt% in the spheres. A higher loading amount in the structure may cause partial blocking of the pores and the bigger metal aggregates, which decrease the catalytic performance. We thus set the doping ratio of Fe and Co

* Corresponding authors.
E-mail addresses: duy@njust.edu.cn (Y. Du), jiqingmin@njust.edu.cn (Q. Ji).
[1] These authors contributed equally to this work.

https://doi.org/10.1016/j.cclet.2022.107858
1001-8417/

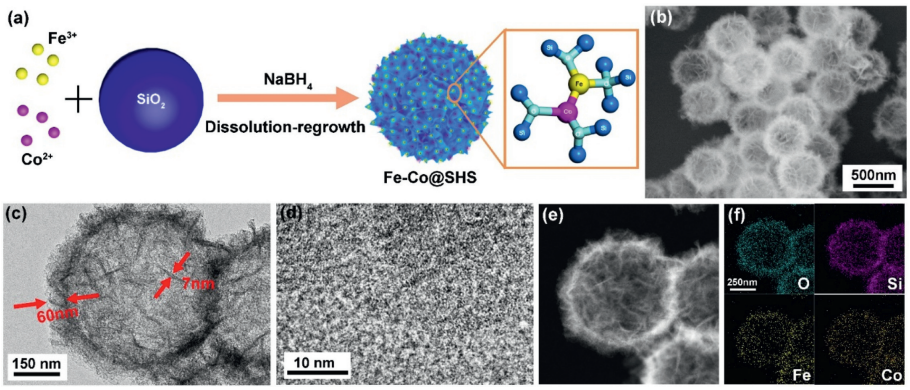

Fig. 1. (a) Scheme for the preparation of Fe-Co@SHS with enhanced peroxidase-like activity. (b) SEM image, (c, d) TEM images of bimetallic Fe-Co@SHS. (e) STEM images and (f) corresponding element mappings of bimetallic Fe-Co@SHS.

to 1:1 with the metal ion concentration of 1 mmol/L in this work. Fig. S1 (Supporting information) shows the appearance of the mixing dispersion of silica particles (30 mg/mL) with Fe (1 mmol/L) and Co ions (1 mmol/L). The dispersion's color (pink yellow) is different from that of the silica particles dispersion (white) and the dispersions with sole Fe ion (pale yellow) or Co ion (light pink). It suggests the well-mixing states of two metal ions with silica particles in the mixture solution. The addition of $NaBH_4$ may change the solution color into black due to the reduction of Fe^{3+} and Co^{2+} into Fe^0 and Co^0 (Fig. S1). After the hydrothermal reaction at 140 °C for 20 h, the solution turns to dark brown color (Fig. S1), which should be due to the formation of Fe(OH)(OOH) and Co(OH)(OOH) in the silica matrix [17]. Fig. S2 (Supporting information) shows the image of the solid silica samples with Fe/Co co-incorporation (Fe-Co@SHS). The powder sample has a brown color, while the samples of Fe@SHS and Co@SHS by a similar fabrication process show pale yellow and light pink colors, respectively.

SEM and TEM investigations on Fe@SHS, Co@SHS, and Fe-Co@SHS indicate the formation of hollow spheres composed of nanosheet networks (Figs. 1b and c, Figs. S3-S5 in Supporting information). The size of the spheres is about 500 nm in diameter and 60 nm in thickness. The silica nanosheets in shells is about 5-10 nm in thickness. We can observe tiny black spots with the size of ~1-2 nm homogeneously distributed on the shell of the spheres in the TEM images (Fig. 1d and Fig. S5). In comparison with the hollow spheres without metal, these tiny black spots should be the aggregates from Fe/Co components in the silica framework. The elemental mapping and the energy-dispersive X-ray (EDX) analyses demonstrate the homogeneous distribution of Fe and Co elements in the structure. (Figs. 1e and f, Fig. S6 in Supporting information).

XRD pattern of Fe-Co@SHS exhibits a broad peak from the amorphous silica around 23° (Fig. 2a). Similar patterns also display for SHS without metal and Fe@SHS or Co@SHS. Diffraction peaks from Fe or Co species can not be observed for Fe@SHS and Co@SHS, which should be due to the too-small aggregate state in the structures beyond the XRD detection limit (>2 nm). It suggests the formation of highly dispersed metal components within the silica matrix by this strategy. A weak diffraction peak at 35.44° appears for Fe-Co@SHS, which can be assigned as cobalt iron oxide (JCPDS No. 22-1086). To further confirm the formation of cobalt iron oxide within the porous silica framework, we carried out the synthesis process by only mixing the Fe and Co ions in the $NaBH_4$ solution. The results prove that the mixture of Fe and Co ions may form cobalt iron oxide after the hydrothermal reaction, which exhibits more obvious diffraction peaks in the XRD spectrum (Fig. S7 in Supporting information). It thus suggests that the co-incorporation of Fe and Co species tends to form $CoFeO_x$ in the silica sphere rather than separated iron or cobalt oxides during the regrowth process of silica.

From the FT-IR spectra of Fe-Co@SHS, Fe@SHS, Co@SHS, and SHS (Fig. 2b), we can find that the broadband for the terminal -OH groups at 3450 cm^{-1} is strengthened for Fe-Co@SHS [18]. And the absorption for the siloxane network around 1100 cm^{-1} is shifted to lower wavenumbers. It suggests the formation of more incomplete silica frameworks with the doping of metals [19,20]. The bending vibration of Si-O-Si around 460 cm^{-1} is also shifted for Fe-Co@SHS, Fe@SHS, and Co@SHS, which might be due to the formation of Si-O-Co or Si-O-Fe [21].

The chemical states and composition of the metals in Fe-Co@SHS were further studied and compared by XPS measurements. The survey spectrum of Fe-Co@SHS clearly shows the presence of O, Si, Fe and Co elements (Fig. S8 in Supporting information). The high-resolution O 1s spectrum can be resolved into four peaks of M-O (530.5 eV), Si-O_x (531.61 eV), Si-O-Si (532.54 eV) and absorbed O (533.75 eV) (Fig. S9 in Supporting information) [22]. Two characteristic peaks at 781.1 eV and 796.7 eV are shown in the Co 2p spectrum of Fe-Co@SHS, corresponding to Co $2p_{3/2}$ and Co $2p_{1/2}$ with satellite peaks (786.62 and 803.15 eV) (Fig. 2c). Their energy spacing of 15.6 eV implies the mixed oxidation state of Co^{2+} and Co^{3+} [23]. According to the deconvoluted peaks for Co^{2+}

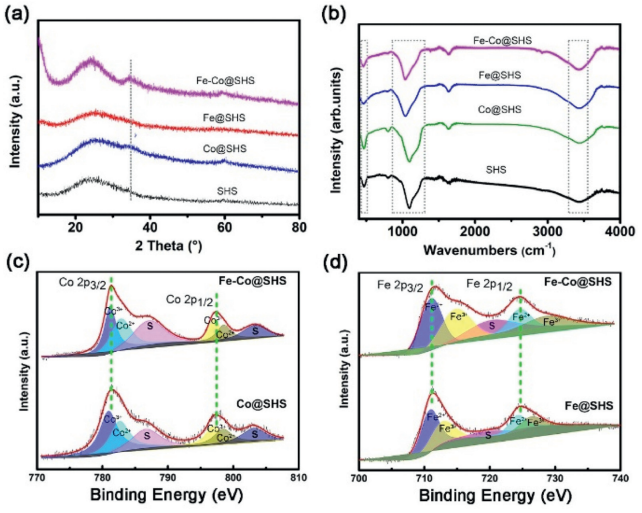

Fig. 2. (a) XRD patterns and (b) FTIR spectra of silica spheres with and without metal incorporation. (c) Co 2p and (d) Fe 2p XPS spectra of silica spheres with metal incorporation.

and Co^{3+}, the percentages of Co^{2+} and Co^{3+} for Fe-Co@SHS are calculated to be 51.80% and 48.20%, respectively. In comparison with Co@SHS, the peak positions are shifted. The Co^{2+}/Co^{3+} ratio also changes to 44.28:55.72. A similar trend is also observed for the Fe 2p spectra of Fe-Co@SHS and Fe@SHS (Fig. 2d). The peaks centered at 711.8 and 725 eV are associated with Fe $2p_{3/2}$ and Fe $2p_{1/2}$, respectively. The broad peak at 720.12 eV is attributed to the satellite peak of Fe. The fitted peaks at 710.83 and 724.23 eV are assigned to Fe^{2+}, while 712.70 and 726. 32 eV are from Fe^{3+} [24,25]. Their percentage contents are 57.84% (Fe^{2+}) and 42.16% (Fe^{3+}) for Fe-Co@SHS, which are different for the values of Fe@SHS (Fe^{2+} 50.86%, Fe^{3+} 49.14%). These results confirm the co-incorporation of Fe and Co in the silica may change the coordination states of the metals and facilitate the formation of cobalt iron oxide. Based on the XPS analysis, we also estimate the metal contents in Fe-Co@SHS, which are 6% for Fe and 7% for Co. The Fe/Co ratio is near 1 and almost the same as the mixing ratio for the preparation of Fe-Co@SHS. This result suggests that the Fe/Co doping ratio in silica hollow spheres should be able to adjust by controlling the mixing ratios during the preparation process. However, to more clearly understand the effect of bimetallic doping, here we only focus on the ratio of 1:1.

The nitrogen sorption analyses were applied to study the influence of the incorporated metals on the porous features of Fe-Co@SHS (Fig. S10). The adsorption-desorption isotherm displays typical type IV with a H3 hysteresis loop. The Brunauer-Emmett-Teller (BET) specific surface area and total pore volume of Fe-Co@SHS are calculated to be 440.20 m^2/g and 0.952 m^3/g. The distribution of pores is in the range of 3-5 nm (Fig. S8). The porous features of Fe-Co@SHS, Co@SHS, Fe@SHS, and SHS are shown in Table S1 (Supporting information). Compared with SHS, the surface areas of metal-doped spheres are increased. The pore distributions also become narrower. It implies that the incorporated metals in the silica framework are not blocked the porous space, and may partially repair the structural defects in the silica matrix, which thus lead to a higher surface area with more even pore size distribution. Fe-Co@SHS possesses a much higher pore volume than that of Co@SHS and Fe@SHS. As the Fe/Co bimetallic doping leads to the formation of relatively larger $CoFeO_x$ crystals, it thus may induce larger pore space and bigger changes in the silica frameworks, which should favor the access to external molecules.

The activity of the doped metals in Fe-Co@SHS is evaluated based on the oxidation process of 3,3′,5,5′-tetramethylbenzidine (TMB) with H_2O_2, which changes to a blue color with major absorption peaks at 370 and 652 nm in the UV-Vis spectrum (Fig. 3a). From the time-dependent intensity changes at 652 nm (Fig. 3b), the catalytic activities of various metal-incorporated silica spheres are compared. Fe-Co@SHS exhibits much higher activity than that of Co@SHS and Fe@SHS. Since the catalytic process shows color change, the performance can also detect directly by bare eyes (Fig. 3a inset). We can directly distinguish the efficiency order of Fe-Co@SHS > Fe @SHS > Co@SHS.

To further understand the peroxidase-like catalytic activity of Fe-Co@SHSs, the steady-state kinetic analysis is carried out according to the variations of TMB and H_2O_2 concentrations (Figs. S11a and c in Supporting information). The steady-state kinetic parameters of Michaelis constant K_m and maximal reaction velocity V_{max} are estimated by the Lineweaver-Burk double reciprocal plots (Figs. S11b and d in Supporting information). K_m is related to the binding capacity of the enzyme and its substrates, while V_{max} means the maximal reaction rate at saturating substrate concentration. The K_m value of Fe-Co@SHS is 0.056 mmol/L for TMB and 0.10 mmol/L for H_2O_2, respectively, which is much lower than that of peroxidase from horseradish enzyme (HRP) (Table S2 in Supporting information). The lower K_m value means a stronger affinity between the nanozyme and substrates. The V_{max} value of Fe-Co@SHS is also much higher than HRP and other supported Fe/Co nanocatalysts (Table S2).

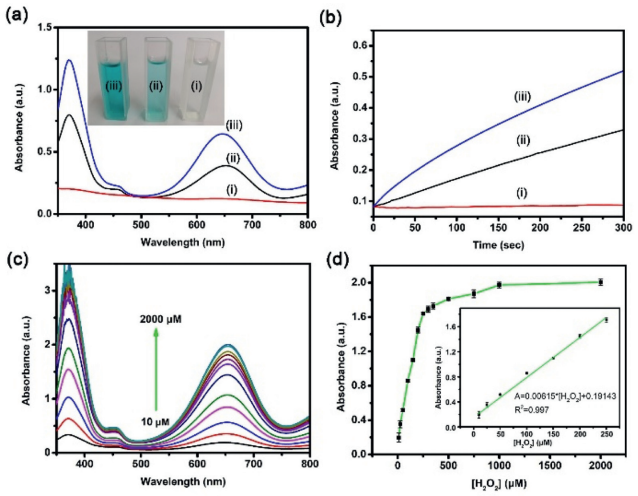

Fig. 3. (a) Absorption spectra for the oxidation of TMB by using different silica spheres with metals as catalysts under 25 °C for 5 min. The inset image is the appearance of reaction solutions. (b) Time-dependent absorbance of TMB at $\lambda = 652$ nm varied with different silica spheres with metals as catalysts. (i) Co@SHS, (ii) Fe@SHS, and (iii) Fe-Co@SHS. (c) UV-vis spectra recording the oxidation of TMB catalyzed by Fe-Co@SHS in the presence of H_2O_2 with varied concentrations. (d) The relation curve between the absorbance at 652 nm and H_2O_2 concentration. The inset is the linear calibration plot for H_2O_2 detection.

The pH value and temperature of the reaction may also influence the catalytic efficiency of Fe-Co@SHS. The optimal reaction condition is shown at pH 2 and 45 °C (Fig. S12 in Supporting information). It is worth noting that Fe-Co@SHS is not sensitive to temperature, while natural enzymes always have the optimal temperature for the highest activity. It means that Fe-Co@SHS may act as a more stable nanozyme with enhanced peroxidase-like activity compared with peroxidases.

The excellent catalysis performance of Fe-Co@SHS should be due to the synergistic effect of the incorporated Fe and Co. Based on the Fenton-type reaction mechanism [26,27], H_2O_2 can simultaneously react with M^{2+} (M = Fe and Co) to produce reactive oxidative species (ROS) of $^{\bullet}OH$ and $^{\bullet}OOH$ radicals as shown in Eqs. 1 and 2 [28,29]. The colorless TMB is then oxidized by $^{\bullet}OH$ to generate blue ox-TMB (equation III). As the standard redox potential of Fe^{3+}/Fe^{2+} (0.77 V) is lower than that of Co^{3+}/Co^{2+} (1.81 V), it means that Co^{3+} could be reduced by Fe^{2+} through equation IV [30,31]. It thus may accelerate the formation of reactive species continuously in the catalytic cycle and improve the catalytic efficiency (Fig. S13 in Supporting information).

$$M^{2+} + H_2O_2 \rightarrow M^{3+} + {}^{\bullet}OH + OH^- \quad (1)$$

$$M^{3+} + H_2O_2 \rightarrow M^{2+} + {}^{\bullet}OOH + H^+ \quad (2)$$

$$^{\bullet}OH + TMB \rightarrow TMB\ (oxidized) \quad (3)$$

$$Fe^{2+} + Co^{3+} \rightarrow Fe^{3+} + Co^{2+} \quad (4)$$

Considering the outstanding peroxidase-like activity of Fe-Co@SHS to react with H_2O_2, we use Fe-Co@SHS to construct the colorimetric detection system of H_2O_2 (Figs. 3c and d). H_2O_2 is a reactive oxygen species and a by-product of many oxidative biological reactions [32,33]. Therefore, the detection of H_2O_2 is essential

to study physiological or biomedical processes and monitor biochemical processes. The colorimetric sensing system has been regarded as a very effective and promising detection method due to the rapid visual response and facile operation [34–37]. It should note that Fe-Co@SHS is the first example of a silica-supported Fe-Co bimetallic nanozyme for H_2O_2 detection. Under the optimized conditions (pH 2 and $T = 45$ °C), the absorbance intensity at 652 nm is linearly proportional to the concentration of H_2O_2 in the range of 10-250 μmol/L (inset in Fig. 3d). The detection limit for H_2O_2 is calculated to be 0.36 μmol/L (0.012 ppm) (Fig. S14 in Supporting information). Fe-Co@SHS also exhibits a better detection performance on H_2O_2 than other supported metal nanozymes (Table S3 in Supporting information).

In summary, we fabricated bimetallic Fe-Co@SHSs with a new distribution state by a facile one-pot hydrothermal process. Based on the dissolution-regrowth process of silica, Fe and Co are intercalated in the silica framework of hollow spheres with keeping accessibility to external molecules. Due to the synergistic effect of the two metals, the Fe-Co@SHS exhibits remarkably enhanced peroxidase-like activity compared with the monometallic spheres of Fe@SHS and Co@SHS. When used for constructing a colorimetric sensor for the detection of H_2O_2, a low detection limit (0.012 ppm) and wide concentration range (10-250 μmol/L) are achieved. This fabrication strategy can also be explored for the formation of three-metals or four-metals doped hollow spheres (Fig. S15 in Supporting information). The multi-metal doped spheres may be used in other catalytic systems or explored for other potential applications for clinical diagnostics, the monitoring of the environment and food safety, *etc*.

Declaration of competing interest

The authors declare that they have no known competing financial interests or personal relationships that could have appeared to influence the work reported in this paper.

Acknowledgments

Thank for the financial supports from the Instrument & Equipment Open Funding of Nanjing University of Science and Technology; National Natural Science Foundation of China (No. 21875108) and the Fundamental Research Funds for the Central Universities (No. 30921013106).

Supplementary materials

Supplementary material associated with this article can be found, in the online version, at doi:10.1016/j.cclet.2022.107858.

References

[1] C.G. Liu, Y.H. Han, J.T. Zhang, et al., Chem. Eng. J. 370 (2019) 1188–1199.
[2] R.K. Kankala, H. Zhang, C.G. Liu, et al., Adv. Funct. Mater. 29 (2019) 1902652.
[3] G. Wang, H. Zhang, Q. Zhu, et al., J. Catal. 351 (2017) 90–94.
[4] T. Chen, Z. Shi, G. Zhang, et al., ACS Appl. Mater. Interfaces 10 (2018) 42475–42483.
[5] M. Chai, X. Liu, L. Li, et al., Chin. J. Catal. 38 (2017) 1338–1346.
[6] H. Yang, L. Xu, M. Chen, et al., Micropor. Mesopor. Mater. 302 (2020) 110250.
[7] N. Farhadian, S. Liu, A. Asadi, M. Shahlaei, S. Moradi, J. Mol. Liq. 321 (2021) 114896.
[8] J. Wisniewska, I. Sobczak, M. Ziolek, Chem. Eng. J. 413 (2021) 127548.
[9] J. Wang, C. Liu, I. Hussain, et al., RSC Adv. 6 (2016) 54623–54635.
[10] Q. Sun, X. Fu, R. Si, C.H. Wang, N. Yan, ChemCatChem 11 (2019) 5093–5097.
[11] L. Xu, F. Cui, J. Zhang, et al., Nanoscale 10 (2018) 9460–9465.
[12] S. Li, D. Gong, H. Tang, et al., Chem. Eng. J. 334 (2018) 2167–2178.
[13] J. Yang, D. Zeng, J. Li, et al., Chem. Eng. J. 404 (2021) 126376.
[14] Q. Ji, C. Guo, X. Yu, et al., Small 8 (2012) 2345–2349.
[15] Q. Ji, S. Ishihara, T.G. Terentyeva, et al., Chem. Asian J. 10 (2015) 1379–1386.
[16] W. Zhao, J. Sun, Q. Tang, et al., Appl. Surf. Sci. 507 (2020) 144919.
[17] W. Zhao, Y. Fu, Y. Chen, et al., Micropor. Mesopor. Mater. 312 (2020) 110704.
[18] C. Wang, F. Shang, X. Yu, J. Guan, Q. Kan, Appl. Surf. Sci. 258 (2012) 6846–6852.
[19] G. Feng, J. Wang, M. Boronat, et al., J. Am. Chem. Soc. 140 (2018) 4770–4773.
[20] X. Liang, R. Yang, G. Li, C. Hu, Micropor. Mesopor. Mater. 182 (2013) 62–72.
[21] P. Shao, J. Tian, X. Duan, et al., Chem. Eng. J. 359 (2019) 79–87.
[22] Z. Xu, J. Yu, G. Liu, et al., Dalton Trans. 42 (2013) 10190–10197.
[23] P.W. Menezes, A. Indra, V. Gutkin, M. Driess, Chem. Commun. 53 (2017) 8018–8021.
[24] J.V. Coelho, M.S. Guedes, R.G. Prado, et al., Appl. Catal. B: Environ. 144 (2014) 792–799.
[25] H. Chen, Y. Liu, T. Cai, et al., ACS Appl. Mater. Interfaces 11 (2019) 28791–28800.
[26] Y. Chen, H. Cao, W. Shi, H. Liu, Y. Huang, Chem. Commun. 49 (2013) 5013–5015.
[27] Q. Chen, X. Zhang, S. Li, H. Liu, Y. Huang, Chem. Eng. J. 395 (2020) 125130.
[28] X. Dang, H. Zhao, Talanta 210 (2020) 120678.
[29] P. Hong, Y. Li, J. He, et al., Appl. Surf. Sci. 526 (2020) 146557.
[30] C. Cai, H. Zhang, X. Zhong, L. Hou, J. Hazard. Mater. 283 (2015) 70–79.
[31] C. Cai, H. Zhang, X. Zhong, L. Hou, Water Res. 66 (2014) 473–485.
[32] A.A. Abd-Elghaffar, A.E. Ali, A.A. Boseila, M.A. Amin, Vaccine 34 (2016) 798–802.
[33] Y. Dong, J. Zheng, Chem. Eng. J. 392 (2020) 123690.
[34] Z. Hu, Z. Dai, X. Hu, et al., J. Nanobiotechnol. 17 (2019) 1–10.
[35] H. Liu, Y. Ding, B. Yang, et al., Sensor. Actuat. B: Chem. 271 (2018) 336–345.
[36] S. Chen, X. Hai, X.W. Chen, J.H. Wang, Anal. Chem. 86 (2014) 6689–6694.
[37] N.G. Hajiagha, A. Mahmoudi, M.R. Sazegar, M.M. Pouramini, Micropor. Mesopor. Mater. 274 (2019) 43–53.